Synthesis of a carbon@Rectorite nanocomposite adsorbent by a hydrothermal carbonization process and their application in the removal of methylene blue and neutral red from aqueous solutions

Huang Yang[a,b], Liu Weijun[a], Wang Weiqing[a,b,*], Feng Qiming[a,b], Liu Jing[a,b]

[a]*School of Environmental Engineering and Resources, Southwest University of Science and Technology, Mianyang 621010, China,*
Tel./Fax: +86 816 6089453; emails: swusthy@163.com *(H. Yang), email:* 408335658@qq.com *(L. Weijun),*
swustwwq@sohu.com *(W. Weiqing),* fengqiming@swust.edu.cn *(F. Qiming),* Liujing-vip@163.com *(L. Jing)*
[b]*Laboratory of Solid Waste Treatment and Resource Recycle, Ministry of Education, Mianyang 621010, China, Tel. +86 816*
2419223; Fax: +86 816 2419492

ABSTRACT

Carbon@REC nanocomposite (C@REC) was synthesized by a hydrothermal carbonization process, and characterized by XRD, Fourier transform infrared spectroscopy, thermal gravimetric analysis, SEM, nitrogen adsorption–desorption measurements, and zeta potential analysis. The adsorption property of the C@REC was investigated as a function of pH of solution, adsorbent dosage, contact time, and initial concentration of MB and NR. The results suggest that amorphous carbon supported on the surface of rectorite. The adsorption experiment showed that adsorption kinetics of MB and NR onto the followed the pseudo-second-order kinetic model. The adsorption isotherm data were fitted well to the Langmuir isotherm. The adsorption capacities for the removal of MB and NR on the C@REC determined using the Langmuir equation were 15.68 and 20.30 mg g^{-1}, respectively.

Keywords: Rectorite; Carbon; Methylene blue; Neutral red; Adsorption

1. Introduction

Cationic dyes are widely used in industries such as textiles, rubber, paper, plastic, and cosmetics. Therefore, large amount of colored wastewater is produced. Because the release of colored wastewater from these industries may present an eco-toxic hazard, it is of great importance to provide waste treatment facilities for minimizing these substances in the effluents before discharge [1]. There are some technologies available for treatment of dye-containing wastewater, such as biodegradation [2,3], chemical oxidation [4], photo degradation [5], electrochemical degradation [6] and adsorption [7,8]. Among those techniques, the most common one is adsorption technology due to its effectiveness, efficiency, economy, and no secondary pollution. Commonly, adsorbents are used to remove dye wastewater, including carbon [9], zeolites [10], clays [11,12]. However, there are still some disadvantages, such as low adsorption capacity, long adsorption time, and separation inconvenience, which limit their applications in dye wastewater treatment.

Carbonaceous materials have some advantages as adsorbent for contaminant removal from aqueous

*Corresponding author.

solutions, such as high removal efficiency, simple operation, and low cost. At present, hydrothermal carbonization (HTC) of biomass has been an important route for preparing carbonaceous materials [13,14]. Several carbonaceous materials have been synthesized by HTC and applied to adsorb the organic dyes or heavy metal ions pollutants. For example, H.W. Liang et al. fabricated that the carbonaceous nanofiber membranes can effectively remove the methylene blue (MB), Cr(VI), and Pb(II) [15]. A. Jain et al. prepared a kind of high-surface area mesoporous activated carbons using HTC of coconut shell and used it to remove rhodamine B [16]. Qi Zhou and Chen et al. reported that attapulgite@carbon nanocomposite performed as a high-efficient adsorbent for removal of organic dyes and heavy metal ions [17,18]. Wu et al. one magnetic mesoporous carbon microsphere was synthesized using carboxymethylcellulose and nickel acetate [19].

The rectorite is a sort of regularly interstratified clay mineral with alternate pairs of dioctahedral mica-like layer (nonexpansible) and dioctahedral smectite-like layer (expansible) existing in 1:1 ratio. Like the montmorillonite, rectorite was widely used as adsorption material because of large surface areas, high cation-exchange capacity and low cost [20]. Therefore, we designed and prepared the eco-friendly biomass-derived carbon loaded on the surface of rectorite by hydrothermal synthesis. The prepared Carbon@rectorite nanocomposite (C@REC) was characterized by X-ray diffraction (XRD), Fourier transform infrared spectroscopy (FT-IR), thermal gravimetric analysis (TGA), scanning electron microscope (SEM), nitrogen adsorption–desorption measurements, and zeta potential analysis.

In this study, two kinds of the cationic dyes, MB and neutral red (NR), were selected as adsorbates.

The objective of the study was to evaluate the adsorption potential of C@REC for MB and NR removal. The effects of various factors on the adsorption such as initial pH, adsorbent dosage, contact time, and initial dye concentration have been studied in this study. The equilibrium and kinetic data of the adsorption studies were processed to understand the adsorption mechanism of MB and NR onto C@REC.
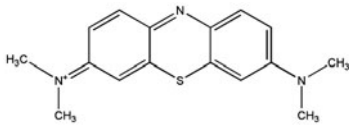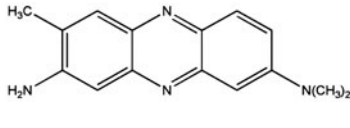
2. Materials and methods

2.1. Materials

All chemical reagents were of analytical grade and used as received without further purification. Glucose, MB, and NR were purchased from Tianjin Kermel chemical reagent Co., China. Rectorite was purchased from Hubei Zhongxiang Rectorite Mine (Wuhan, China). The properties characteristics of MB and NR are listed in Table 1.

2.2. Preparation of C@REC

C@REC was obtained by hydrothermal synthesis method [23]. Five grams of glucose was dissolved in 70 mL of ultrapure water at room temperature. One gram of rectorite was then added to above solution and sonicated for 10 min to form a homogeneous dispersion. The mixture solution was transferred into a Teflon-lined stainless steel autoclave and heated at 180°C for 6 h. After the heat treatment, the autoclave was allowed to cool naturally to room temperature, and the products were rinsed with distilled water and ethanol when filtered by Buchner funnel. They were then dried in an oven at 60°C for 24 h. The final products were ground in an agate mortar and kept in a desiccator.

Table 1
Properties and characteristics of MB and NR [21,22]

Generic name	MB	NR
Chemical name (IUPAC)	3,7-bis(Dimethylamino)-phenazathionium chloride tetramethylthionine chloride	3-Amino-7-dimethylamino-2-methylphenazine hydrochloride
Chemical formula	$C_{16}H_{18}ClN_3S \cdot 3H_2O$	$C_{15}H_{17}ClN_4$
Molecular weight (g mol^{-1})	373.90	288.78
λ_{max} (nm)	665	529
Color index number	52 015	50 040
Chemical structure		

2.3. Characterization of adsorbent

All characterizations were carried out at room temperature after the complex was changed into fine powder by grinding. The phase identification of sample was examined using PA Nalytical, X'pert PRO XRD. FT-IR spectrum was acquired by Perkin Elmer FT-IR, the spectrum ranged from 4,000–400 cm^{-1}. Morphology analysis was performed on Cambridge, Stereoscan 440 SEM. Zeta potential of the materials was determined by microelectrophoresis using Malven, Zetasizer Nano Zs90 zeta potential analyzer. The zeta potentials of the materials suspensions containing 0.5% solid in 0.01 mol L^{-1} NaNO$_3$ were determined at various pH values. A nitrogen adsorption system (Quantachrome, Autosorb-1MP) was employed to record the adsorption–desorption isotherms at the liquid nitrogen temperature of 77 K.

2.4. Adsorption experiments

For each adsorption experiment, C@REC, MB and NR solution of known concentration were transferred in 100-mL flask, and shaken at 25°C controlled shaker at a constant speed of 150 rpm with a required adsorption time and required pH. The effects of solution initial pH values, adsorbent dosage, contact time, and initial MB and NR concentrations were investigated. The effect of pH was performed by dispersion of 0.1 g of nanocomposite in 25 mL of organic dyes solution of 100 mg L^{-1}. Effect of solution pH on adsorption of MB was investigated in the range of 2.0–10.0, and NR in the range of 1.0–5.0 by the addition of 0.1 mol L^{-1} H$_2$SO$_4$ or 0.1 mol L^{-1} NaOH solutions. The suspensions were shaken in a temperature-controlled shaker at 25°C for 360 min. The adsorbent dosage was changed from 0.5 to 8 g L^{-1} in order to investigate the influence of adsorbent dosage of organic dyes by the composites. Experiments were carried out when initial MB and NR concentrations were 100 mg L^{-1} at 25°C for 360 min, initial pH values were 6.0 and 5.0 ± 0.1, respectively. The adsorption kinetics was determined by analyzing adsorption capacity from the aqueous solution at different time intervals. Experiments were carried out when initial MB and NR concentration were 100 mg L^{-1} at 25°C, initial pH values were 6.0 and 5.0 ± 0.1, respectively. For adsorption isotherms, organic dyes solution of different concentrations in the range of 10–100 mg L^{-1} was shaken. The samples were separated from mixture solution by centrifugation with a speed of 4,000 rpm for 10 min. The concentrations of dyes were measured with Thermo Fisher Evolution EV300 UV–visible spectrophotometer at appropriate wavelengths

corresponding to the maximum absorbance of each dye, 662 nm and 529 nm for MB and NR, respectively. The adsorbed amounts (*q*) of organic dyes were calculated by the following equation:

$$q = \frac{(C_0 - C_e) \times V}{m} \tag{1}$$

where C_0 and C_e are the initial and equilibrium concentrations of organic dyes (mg L^{-1}), V is the volume of solution (L), and m is the mass of adsorbent (g). All assays were carried out in triplicate and only mean values were presented.

3. Results and discussion

3.1. Characterization of the adsorbent

XRD patterns of raw rectorite, C@REC, and glucose-derived carbon (GC) are shown in Fig. 1. XRD analysis of raw rectorite revealed that it consisted mainly of rectorite, with kaolinite and pyrophyllite as mineral admixtures. The pattern of GC sample exhibited broad peaks at $2\theta = 21°$, suggesting that GC sample had low degree of crystallization. As shown in Fig. 1(b), the C@REC contained the characteristic peaks of rectorite, which meant that the process of combination did not change phases of rectorite. The crystallinity of GC was too low, so it was difficult to find it in the C@REC.

The FT-IR spectra of the raw rectorite, C@REC, and GC are presented in Fig. 2. The main bands observed in the FT-IR spectrum of raw rectorite (Fig. 2(a)) were in accordance with a previous report [24]. The peaks at 3,644 and 3,440 cm^{-1} were attributed to the bending vibration of hydrogen band of interlaminar water and the hydroxyl stretching of Si–OH in the FT-IR spectra of rectorite. Water bend band appeared at 1,638 cm^{-1}. The peaks at 1,025 cm^{-1} were associated with the Si–O stretching vibration, while the peaks 450–550 cm^{-1} were assigned to the Si–O bending vibration. After rectorite was coated with carbonaceous components, several new bands, including the 1,400 cm^{-1} bands of carbonyl groups, and the 1,637 cm^{-1} band of C=C, emerge in the FT-IR spectrum of the C@REC nanocomposite. These results indicate that the rectorite has been successfully modified by the functional carbonaceous species.

The successful coating of carbon onto rectorite was further confirmed by TGA performed under air atmosphere. The mass loss curves for raw rectorite, C@REC and GC are shown in Fig. 3. For raw rectorite, the weight losses below 120°C and at about 300°C are
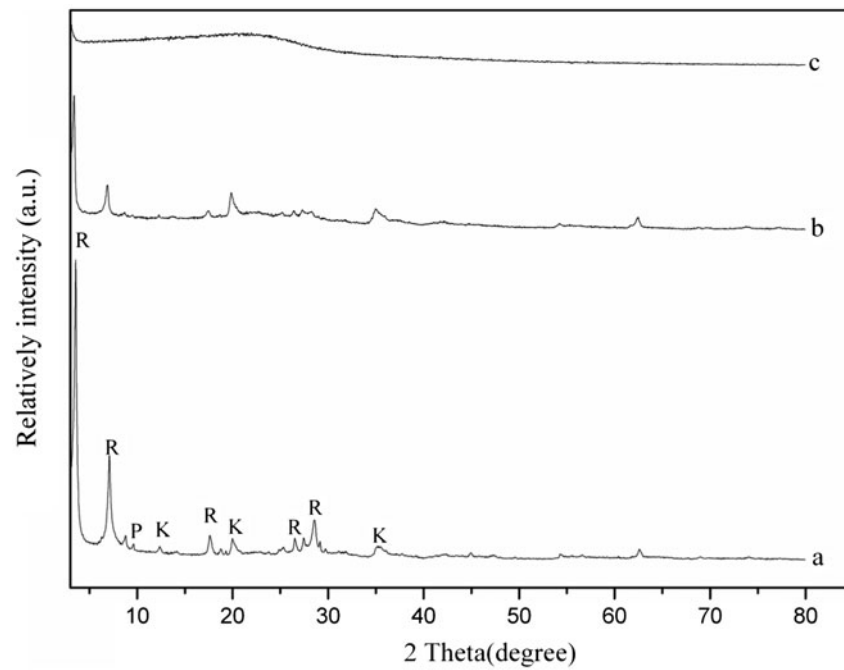
Fig. 1. XRD patterns of (a) raw rectorite, (b) C@REC, and (c) GC (R: rectorite; K: kaolinite; P: pyrophyllite).
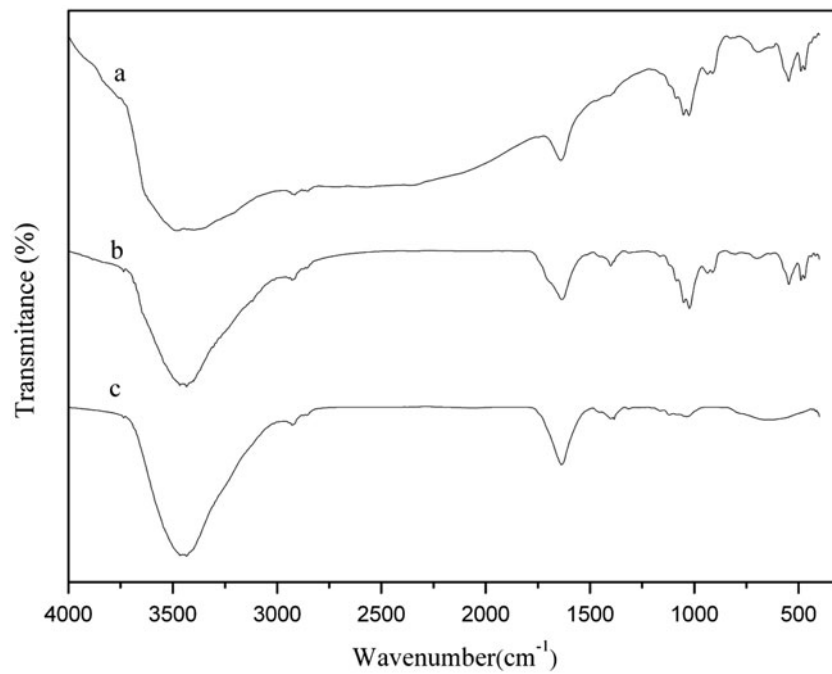

Fig. 2. FT-IR spectra of (a) raw rectorite, (b) C@REC, and (c) GC.

assigned to the release of free water and the structural water of rectorite, respectively. For the C@REC, the main weight loss below 300°C is similar to that of rectorite, but that between 300 and 550°C can be assigned to the oxidative degradation of the carbonaceous nanocomposite under air atmosphere. The weight of C@REC remains almost constant above 550°C owing to the disappearance of carbon species in the nanocomposite, which approximately hold a proportion of 50 wt% as calculated from TGA analysis. The above results further reveal that the GC has been successfully grafted onto the rectorite.

The zeta potentials of the C@REC at various pH values are shown in Fig. 4. For comparison, zeta potentials of rectorite and GC are also included. These results showed that the zeta potential values of the surface of the raw rectorite, C@REC, and GC are negative over the entire pH range from 2.0 to 11.0. The zeta potential value of C@REC is even more negative than those of rectorite at a higher pH value, which may be attributed to the fact that some of the carboxylic groups are located on the surface of the C@REC. The zeta potential value of C@REC is negative, which plays an important role in retaining the cation contaminants.

The microstructure and morphology of the as-prepared samples were observed by SEM. It can be seen from Fig. 5(a) that raw rectorite appear an aggregated morphology with the thin and flexible plate-like shapes. Interestingly, C@REC (Fig. 5(b)) exhibits distinct morphology compared with the raw rectorite, where most of the carbonaceous compounds cover firmly on the surface of rectorite.

Fig. 6 shows the N_2 adsorption–desorption isotherms of C@REC, and the further analysis of the pore size distribution of the micropores and mesopores are shown in the insets of the Fig. 6. N_2 adsorption–desorption isotherm curve of the C@REC nanocomposite is types II isotherms (in the IUPAC classification). The calculated Brunauer–Emmett–Teller (BET) surface area of the nanocomposite is found to be 48.75 $m^2\,g^{-1}$. According to the Horvath–Kawazoe (HK) method, the total micropore volume is 0.295 $cm^3\,g^{-1}$, the micropore size is in the range of 0.3775–1.9325 nm. From the Barrett–Joyner–Halenda (BJH) graph (the inset figure), the pore volume and average pore diameter are estimated to be 0.788 $cm^3\,g^{-1}$ and 12.81 nm, respectively.

3.2. Adsorption of MB and NR onto nanocomposite

The initial pH values of the MB and NR solution are important parameter, which control the adsorption process, particularly the adsorption capacity. We know that the color of NR change from red to yellow in the pH range of 6.8–8.0. So the initial pH values of
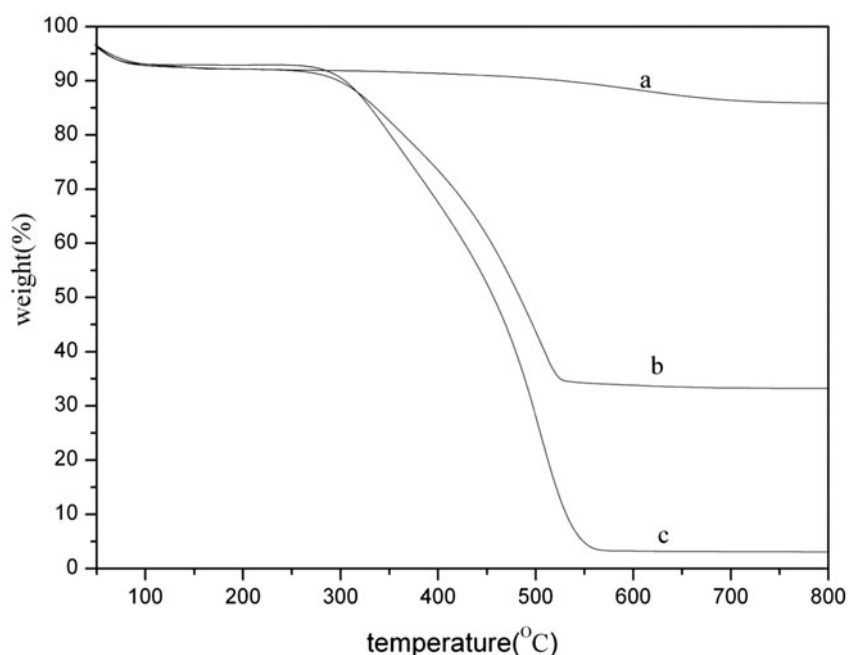

Fig. 3. TGA curves obtained in air for (a) raw rectorite, (b) C@REC, and (c) GC.
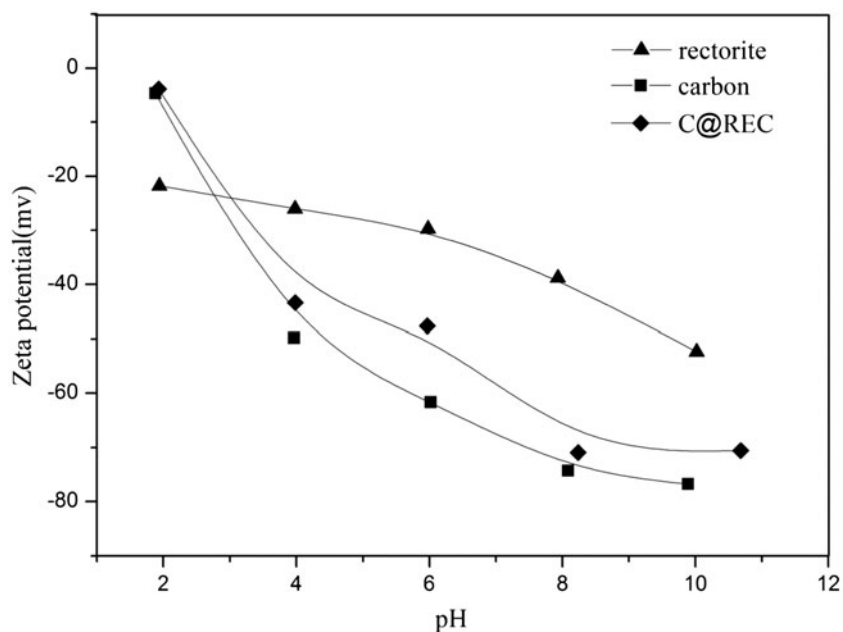
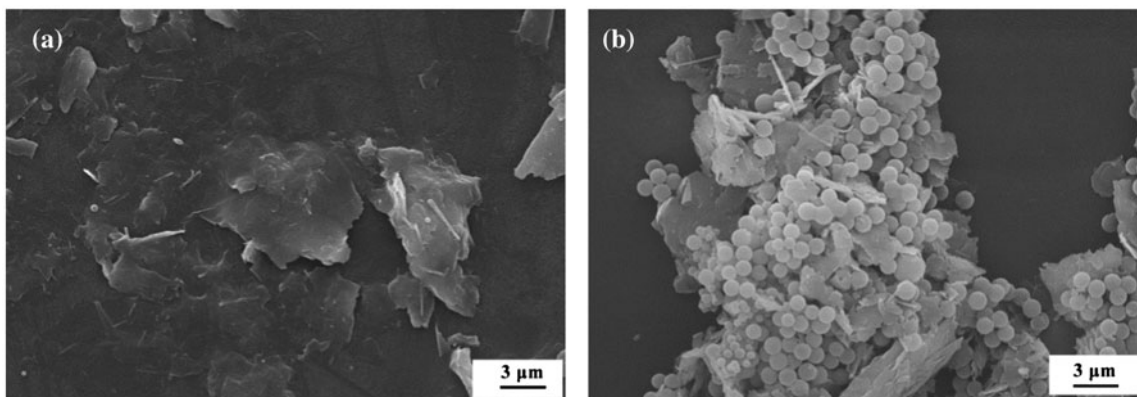Fig. 4. Zeta potentials of the raw rectorite, C@REC, and GC.

Fig. 5. SEM images of (a) raw rectorite and (b) C@REC.

the NR solution were adjusted as 1.0–6.0. The effects of pH on adsorption of MB and NR by nanocomposite are presented in Fig. 7. It can be seen that, with the increase in initial pH values of aqueous solution, the adsorption capacities of MB and NR increase. The electrostatic attraction appeared between negative charged C@REC and cationic MB or NR molecules, which should be responsible for the excellent performance for MB and NR adsorption. At lower pH, the MB and NR had to compete with hydrogen ions among the exchange sites. However, with increasing pH, the competition decreased and the positively charged MB and NR could be adsorbed at the

negatively charged sites on the composites, due to strong electrostatic attraction forces. Furthermore, the adsorption capacity of NR was higher than MB, which may be attributed to NR with smaller the molecular weight and molecular size.

Adsorbent dosage is another important parameter affecting ion adsorption efficiency. Fig. 8 displays the effect of adsorbent dosage on the MB and NR adsorption by nanocomposite. The removal efficiency increased from 11.15 to 90.63% for MB, and increased from 21.79 to 99.99% for NR, when the adsorbent dosage increased from 0.5 to 8 g L^{-1}. However, the adsorption capacity of MB and NR decreased when the
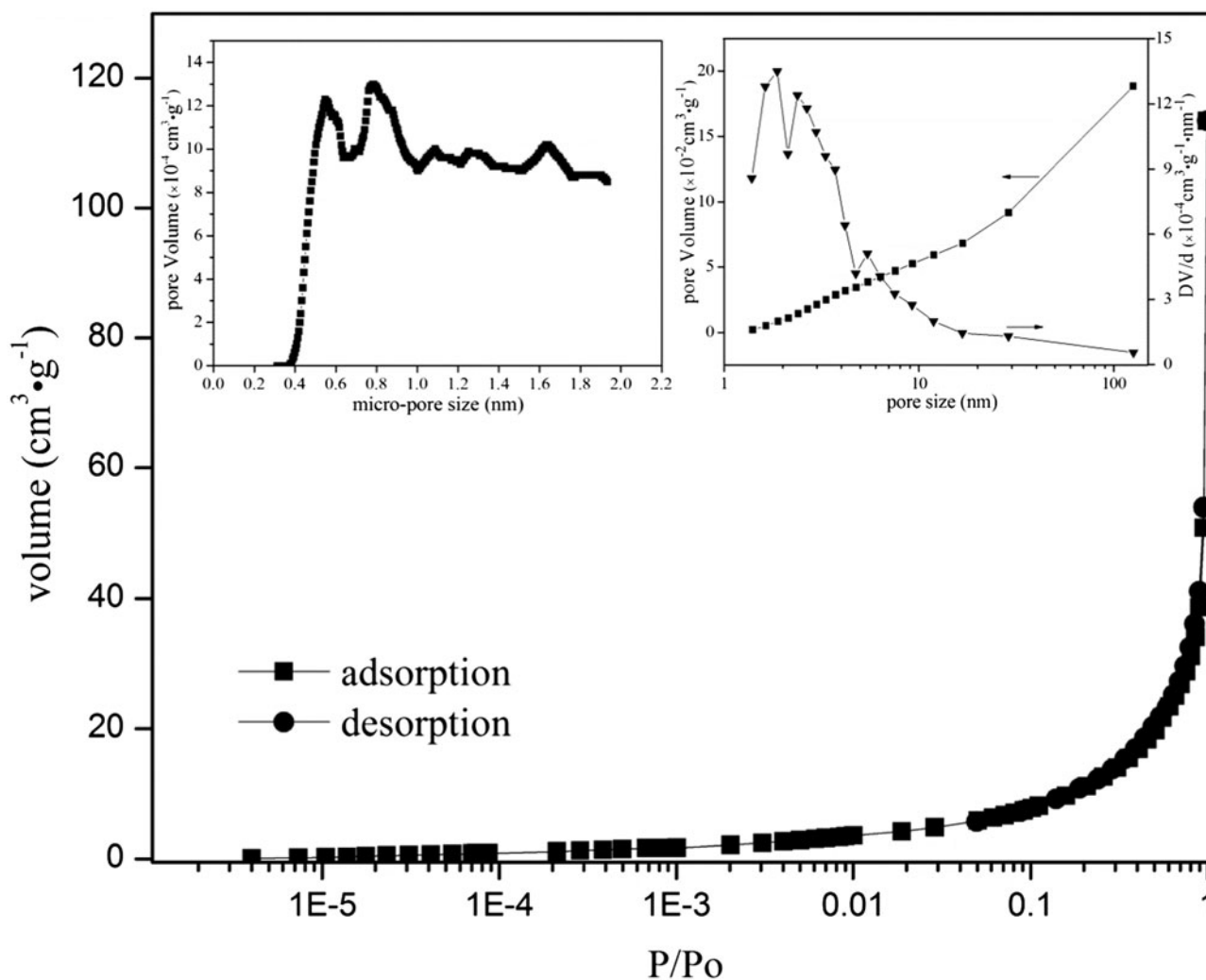
Fig. 6. N$_2$ adsorption–desorption isotherms of C@REC. The inset figures show the pore size distributions of the micropores and mesopores.

adsorbent dosage increased. The reduction in adsorption capacity may be due to the saturation of the active sites of adsorbent which are involved in the adsorption process indicated that for a constant initial dye concentration, increasing the absorbent dosage provided more functional groups and active sites, thus leading to the increase in the removal efficiency of MB and NR.

Fig. 9 shows the kinetics of the adsorption of organic dyes MB and NR by C@REC. Inspection of the uptake–time curves show that the maximum uptake follows the order NR > MB at all time intervals. The kinetic curve for MB showed that adsorption reached equilibrium after approximately 100 min. NR adsorption reached equilibrium in 180 min, and remained constant until the end of the experiment.

The uptake–time data obtained were treated in the form of two simplified kinetic models including pseudo-first-order and pseudo-second-order. The pseudo-first-order model is expressed as shown in Eq. (2) [25]:

$$\log (q_e - q_t) = \log q_e - \frac{k_1 t}{2.303} \quad (2)$$

where k_1 is the pseudo-first-order rate constant (min^{-1}), q_e and q_t are the amounts of MB and NR adsorbed (mg g^{-1}) at equilibrium and at time t (min). On the other hand, the pseudo-second-order model is expressed as shown in Eq. (3) [26]:
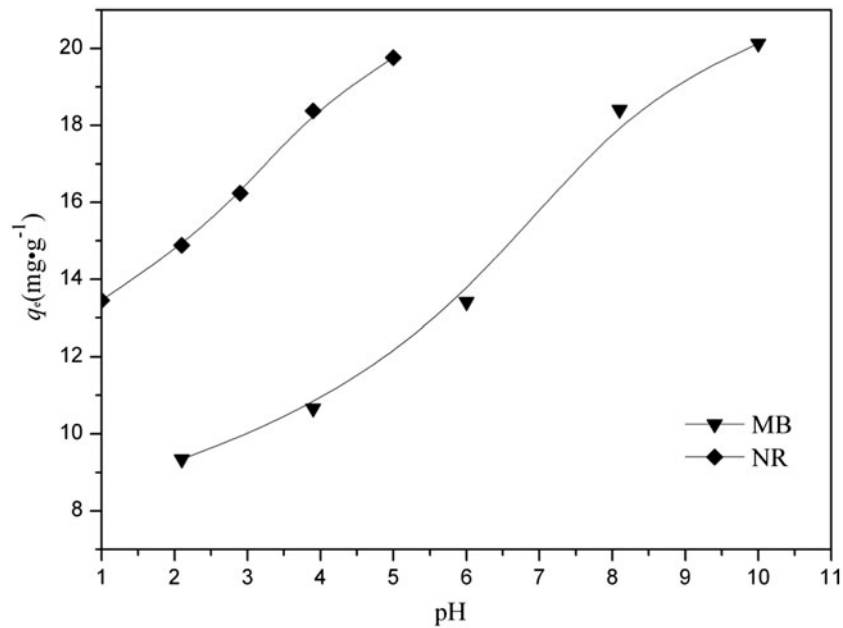
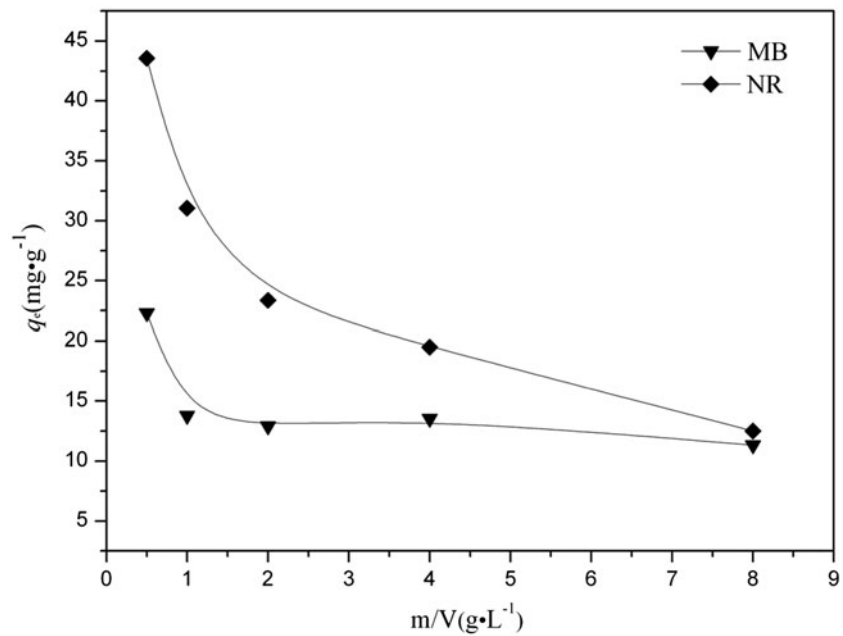Fig. 7. Effect of pH on adsorption of MB and NR onto C@REC.

Fig. 8. Effect of adsorbent dosage on adsorption of MB and NR onto C@REC.

$$\frac{t}{q_t} = \frac{1}{k_2 q_e^2} + \frac{t}{q_e} \qquad (3)$$

where k_2 (g mg^{-1} min^{-1}) is the rate constant of the pseudo-second-order adsorption. The aforementioned

two models basically considering external film diffusion, intraparticle diffusion and interaction step for adsorption process. The rate-determining step of adsorption reaction may be one of the above three steps.
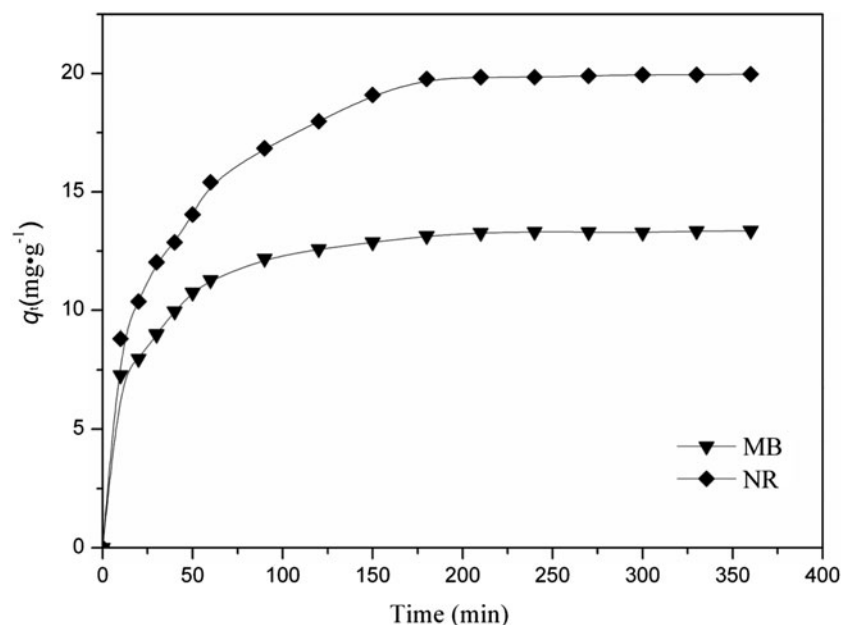
Fig. 9. Effect of contact time on adsorption of MB and NR onto C@REC.

Kinetic constants obtained by linear regression (Fig. 10) for the two models were listed in Table 2. For the pseudo-first-order model, although it showed slightly fitting to the experimental data with the correlation coefficients more than 0.96, the calculated equilibrium adsorption capacities ($q_{e,cal}$) deviated largely from the experimental values ($q_{e,exp}$). In contrast, the high correlation coefficients ($R^2 > 0.99$) were obtained by the pseudo-second-order model. The values of $q_{e,cal}$ also appeared to be very close to the experimentally observed values of $q_{e,exp}$. These results indicate that the pseudo-second-order model is suitable for characterizing the kinetic data.

The relation between the adsorption capacities of the adsorbents and the initial concentrations of two dyes are given by the adsorption isotherm in Fig. 11. It can be observed that the adsorption capacities of the nanocomposite increase with increase in the initial dye concentration. The isotherm data were fitted to the Langmuir and Freundlich isotherms, which are represented by the following equations, respectively [27,28]:

$$\frac{C_e}{q_e} = \frac{1}{bq_m} + \frac{C_e}{q_m} \tag{4}$$

$$\log q_e = \log K_f + \frac{1}{n} \log C_e \tag{5}$$

where constant b is related to the energy of adsorption (L mg^{-1}), q_m is the maximum adsorption capacity (mg g^{-1}), K_f is roughly an indicator of the adsorption capacity, and $1/n$ was the adsorption intensity.

The adsorption isotherm indicates how the adsorption molecules distribute between the liquid phase and the solid phase when the adsorption process reaches an equilibrium state. The analysis of the isotherm data by fitting them to different isotherm models is an important step to find the suitable model that can be used for design purpose [29]. The linear plots of the Langmuir model and Freundlich model are given in Fig. 12(a) and (b). The graphically calculated q_m, b, and R^2 (Langmuir

Table 2
Adsorption kinetic parameters of MB and NR adsorption onto C@REC

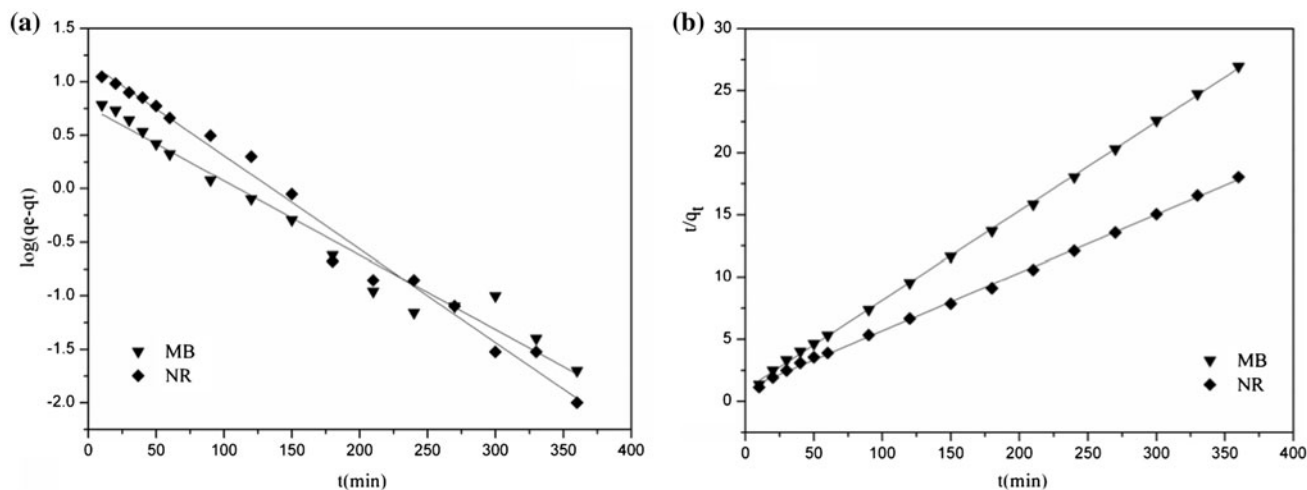| Cationic dyes	Pseudo-first-order				Pseudo-second-order		
	k_1 (min^{-1})	$q_{e,cal}$ (mg g^{-1})	$q_{e,exp}$ (mg g^{-1})	R^2	k_2 (g mg^{-1} min^{-1})	$q_{e,cal}$ (mg g^{-1})	R^2
MB	0.01598	5.85	13.38	0.9687	0.0053	13.94	0.9998
NR	0.02011	15.20	19.98	0.9854	0.0022	21.40	0.9988

Fig. 10. Pseudo-first-order kinetic (a) and pseudo-second-order kinetic and (b) of adsorption MB and NR onto C@REC.
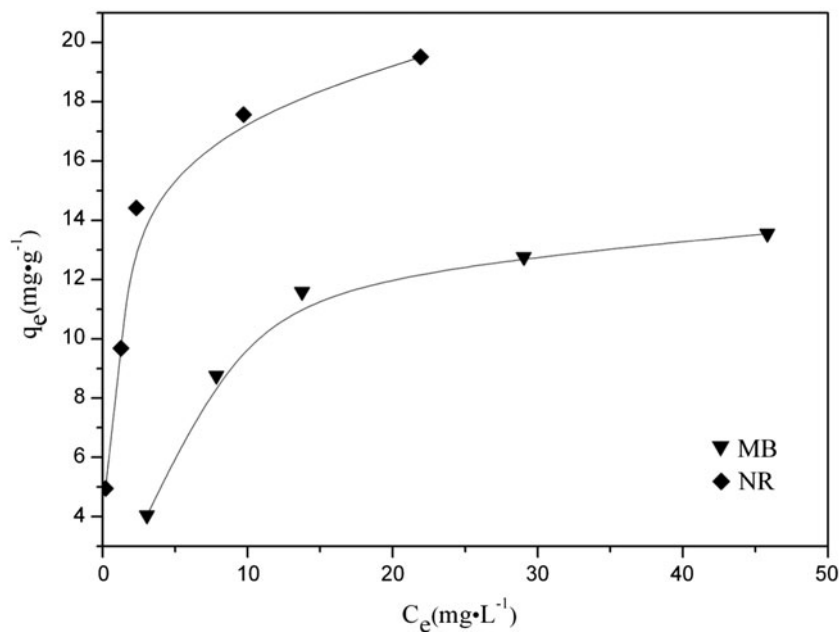

Fig. 11. Equilibrium adsorption isotherms of MB and NR onto C@REC.

isotherm), n, K_f, and R^2 (Freundlich isotherm) were regrouped in Table 3. It can be seen that the values of R^2 of the Langmuir model for the MB and NR are 0.9705 and 0.9977, while the values of R^2 of the Freundlich model for those dyes are 0.8633 and 0.9109, respectively. Therefore, the adsorptions of C@REC nanocomposite followed the Langmuir isotherm model closely, indicating the characteristic of adsorption should be monolayer adsorption process of MB and NR on the nanocomposite with the corresponding monolayer saturated adsorption capacity of 15.68 and 20.30 mg g^{-1}, respectively. The Freundlich model revealed a thermodynamically favorable adsorption of MB and NR onto nanocomposite surface as the Freundlich constants are greater than 2 [30].
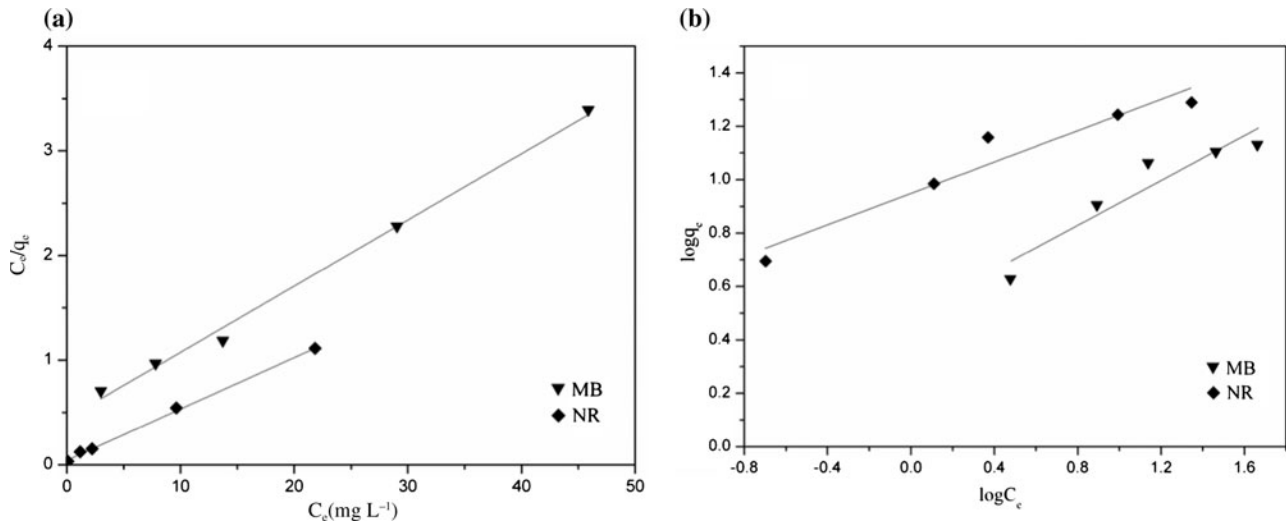
Fig. 12. (a) Langmuir and (b) Freundlich isotherm model fitting curves of MB and NR adsorption on C@REC.

Table 3
Adsorption isotherm parameters of MB and NR adsorption onto C@REC

Cationic dyes	Langmuir equation			Freundlich equation		
	q_m (mg g^{-1})	b (L mg^{-1})	R^2	K_f (mg g^{-1})	n	R^2
MB	15.68	0.1481	0.9705	3.102	2.370	0.8633
NR	20.30	0.9340	0.9977	8.933	3.392	0.9109

Table 4
MB and NR adsorption by other adsorbents

Adsorption capacity (mg g^{-1})	Adsorbents	Refs.
MB		
1.21	Fir wood-based activated carbon	[31]
215.6	Carbonaceous nanofiber membranes	[15]
62.7	Charcoal	[32]
194.2	Carbon@montmorillonite nanocomposites	[23]
9.81	Activated carbon	[33]
13.38	C@REC	This work
NR		
14.9	Zeolite	[34]
37.5	Peanut husk	[35]
54.85	Halloysite nanotube	[36]
25.16	Rice husk	[37]
204.08	Mn-impregnated activated carbons	[38]
19.98	C@REC	This work

3.3. Comparison of various adsorbents

The removal of MB and NR by other adsorbents has been studied extensively, and MB and NR adsorption capacities were reported in literature. Table 4 compares the adsorption capacities of the C@REC with other adsorbents previously used for removal of MB and NR. We find that the adsorption capacities of C@REC for MB and NR are mediocre. However, C@REC is a unique adsorbent because it is low-cost and natural and healthy green material.

4. Conclusions

In this paper, one new C@REC could be synthesized by a one-pot hydrothermal process using two environmentally friendly materials, namely, rectorite clay and glucose. The C@REC showed obvious advantages and possesses high adsorption capacity for the removal of MB and NR in aqueous solution with maximum adsorption capacities of 13.38 and 19.98 mg g^{-1}, respectively. This new nanocomposite was qualified for wastewater treatment as a low-cost, sustainable, effective adsorbent. Furthermore, the surface of a hydrothermal carbon nanolayer could be further engineered or modified to increase its adsorption capability and selectively remove other contaminants in water.

Acknowledgements

References

[1] M.M. Ayad, A.A. El-Nasr, Adsorption of cationic dye (methylene blue) from water using polyaniline nanotubes base, J. Phys. Chem. C 114 (2010) 14377–14383.

[2] O.D. Olukanni, A.A. Osuntoki, D.C. Kalyani, G.O. Gbenle, S.P. Govindwar, Decolorization and biodegradation of Reactive Blue 13 by *Proteus mirabilis* LAG, J. Hazard. Mater. 184 (2010) 290–298.

[3] M. Jonstrup, N. Kumar, M. Murto, B. Mattiasson, Sequential anaerobic–aerobic treatment of azo dyes: Decolourisation and amine degradability, Desalination 280 (2011) 339–346.

[4] G. Ersöz, A. Napoleoni, S. Atalay, Comparative Study using chemical wet oxidation for removal of reactive black 5 in the presence of activated carbon, J. Environ. Eng. 139 (2013) 1462–1469.

[5] A. Turolla, M. Fumagalli, M. Bestetti, M. Antonelli, Electrophotocatalytic decolorization of an azo dye on TiO$_2$ self-organized nanotubes in a laboratory scale reactor, Desalination 285 (2012) 377–382.

[6] C. Cai, H. Zhang, X. Zhong, L. Hou, Electrochemical enhanced heterogeneous activation of peroxidisulfate by Fe-Co/SBA-15 catalyst for the degradation of Orange II in water, Water Res. 66 (2014) 473–485.

[7] C. Kannan, N. Buvaneswari, T. Palvannan, Removal of plant poisoning dyes by adsorption on Tomato Plant Root and green carbon from aqueous solution and its recovery, Desalination 249 (2009) 1132–1138.

[8] S. Yao, S. Song, Z. Shi, Adsorption properties and photocatalytic activity of TiO$_2$/activated carbon fiber composite, Russ. J. Phys. Chem. A 88 (2014) 1066–1070.

[9] K. Sandeep, B. Gaurav, D. Neeraj, U. Ahmad, Multi walled carbon nanotubes as sorbent for removal of crystal violet, J. Nanosci. Nanotechnol. 14 (2014) 7054–7059.

[10] X. Jin, B. Yu, Z. Chen, J.M. Arocena, R.W. Thring Adsorption of Orange II dye in aqueous solution onto surfactant-coated zeolite: Characterization, kinetic and thermodynamic studies, J. Colloid Interface Sci. 435 (2014) 15–20.

[11] I. Feddal, A. Ramdani, S. Taleb, E.M. Gaigneaux, N. Batis, N. Ghaffour, Adsorption capacity of methylene blue, an organic pollutant, by montmorillonite clay, Desalin. Water Treat. 52 (2014) 2654–2661.

[12] S.A. Carolina, I. Nani, I. Suryadi, Adsorption of N-methylated diaminotriphenilmethane dye (malachite green) on natural rarasaponin modified kaolin, Desalin. Water Treat. 41 (2012) 1–3.

[13] B. Hu, K. Wang, L.H. Wu, S.H. Yu, M. Antonietti, M.M. Titirici, Engineering carbon materials from the hydrothermal carbonization process of biomass, Adv. Mater. 22 (2010) 813–828.

[14] B. Hu, S.H. Yu, K. Wang, L. Liu, X.W. Xu, Functional carbonaceous materials from hydrothermal carbonization of biomass: an effective chemical process, Dalton Trans. 40 (2008) 5414–5423.

[15] H.W. Liang, X. Cao, W.J. Zhang, H.T. Lin, F. Zhou, L.F. Chen, S.H. Yu, Robust and highly efficient free-standing carbonaceous nanofiber membranes for water purification, Adv. Funct. Mater. 21 (2011) 3851–3858.

[16] A. Jain, R. Balasubramanian, M.P. Srinivasan, Tuning hydrochar properties for enhanced mesopore development in activated carbon by hydrothermal carbonization, Microporous Mesoporous Mater. 203 (2015) 178–185.

[17] Q. Zhou, Q. Gao, W. Luo, C.J. Yan, Z.N. Ji, P. Duan, One-step synthesis of amino-functionalized attapulgite clay nanoparticles adsorbent by hydrothermal carbonization of chitosan for removal of methylene blue from wastewater, Colloids Surf., A: Physicochem. Eng. Aspects 470 (2015) 248–257.

[18] L.F. Chen, H.W. Liang, Y. Lu, C.H. Cui, S.H. Yu, Synthesis of an attapulgite clay@carbon nanocomposite adsorbent by a hydrothermal carbonization process and their application in the removal of toxic metal ions from water, Langmuir 27 (2011) 8998–9004.

[19] Q. Wu, W. Li, J. Tan, X. Nan, S.X. Liu, Hydrothermal synthesis of magnetic mesoporous carbon microspheres from carboxymethylcellulose and nickel acetate, Appl. Surf. Sci. 332 (2015) 354–361.

[20] Y. Zhao, Z. Shao, C. Chen, J. Hu, H. Chen, Effect of environmental conditions on the adsorption behavior of Sr(II) by Na-rectorite, Appl. Clay Sci. 87 (2014) 1–6.

[21] B.H. Hameed, A.A. Ahmad, Batch adsorption of methylene blue from aqueous solution by garlic peel, an agricultural waste biomass, J. Hazard. Mater. 164 (2009) 870–875.

[22] S. Çoruh, E.H. Gürkan, Adsorption of neutral red from aqueous solutions using waste foundry sand: Full factorial design analysis, Environ. Prog. Sustainable Energy 33 (2014) 1086–1095.

[23] L. Ai, L. Li, Efficient removal of organic dyes from aqueous solution with ecofriendly biomass-derived carbon@montmorillonite nanocomposites by one-step hydrothermal process, Chem. Eng. J. 223 (2013) 688–695.

[24] X.L. Tan, P.P. Chang, Q.H. Fan, X. Zhou, S.M. Yu, W.S. Wu, X.K. Wang, Sorption of Pb(II) on Na-rectorite: Effects of pH, ionic strength, temperature, soil humic acid and fulvic acid, Colloids Surf., A 328 (2008) 8–14.

[25] S. Lagergren, About the theory of so-called adsorption of soluble substances, Kungliga Svenska Vetenskapsakademiens Handlingar 24 (1898) 1–39.

[26] Y.S. Ho, G. McKay, Sorption of dye from aqueous solution by peat, Chem. Eng. J. 70 (1998) 115–124.

[27] I. Langmuir, The Constitution And Fundamental Properties Of Solids And Liquids. Part I. Solids, J. Am. Chem. Soc. 38 (1916) 2221–2295.

[28] H.M.F. Freundlich, On the adsorption in solution, Z. Phys. Chem. 57 (1906) 385–471.

[29] M. El-Guendi, Homogeneous surface diffusion model of basic dyestuffs onto natural clay in batch adsorbers, Adsorpt. Sci. Technol. 8 (1991) 217–225.

[30] R.E. Treybal, Mass Transfer Operations, third ed., McGraw-Hill Companies, New York, NY, 1980.

[31] F.C. Wu, R.L. Tseng, High adsorption capacity NaOH-activated carbon for dye removal from aqueous solution, J. Hazard. Mater. 152 (2008) 1256–1267.

[32] F. Banat, S. Al-Asheh, R. Al-Ahmad, F. Bni-Khalid, Bench-scale and packed bed sorption of methylene blue using treated olive pomace and charcoal, Bioresour. Technol. 98 (2007) 3017–3025.

[33] V.V. Basava Rao, S.R. Ram Mohan Rao, Adsorption studies on treatment of textile dyeing industrial effluent by flyash, Chem. Eng. J. 116 (2006) 77–84.

[34] A. Chojnacki, K. Chojnacka, J. Hoffmann, H. Górecki, The application of natural zeolites for mercury removal: From laboratory tests to industrial scale, Miner. Eng. 17 (2004) 933–937.

[35] H.A. El-Maghraby, Removal of a basc dye from agueous solution by adsorption using rice hulls, Global Nest J. 13 (2011) 90–98.

[36] P. Luo, Y. Zhao, B. Zhang, J. Liu, Y. Yang, J. Liu, Study on the adsorption of Neutral Red from aqueous solution onto halloysite nanotubes, Water Res. 44 (2010) 1489–1497.

[37] W.H. Zou, P. Han, Y.L. Li, X. Liu, X.T. He, R.P. Han, Equilibrium, kinetic and mechanism study for the adsorption of neutral red onto rice husk, Desalin. Water Treat. 12 (2009) 210–218.

[38] J. Zhang, Q.Q. Shi, C.L. Zhang, J.T. Xu, B. Zhai, B. Zhang, Adsorption of Neutral Red onto Mn-impregnated activated carbons prepared from *Typha orientalis*, Bioresour. Technol. 99 (2008) 8974–8980.